

**Supplemental Information**

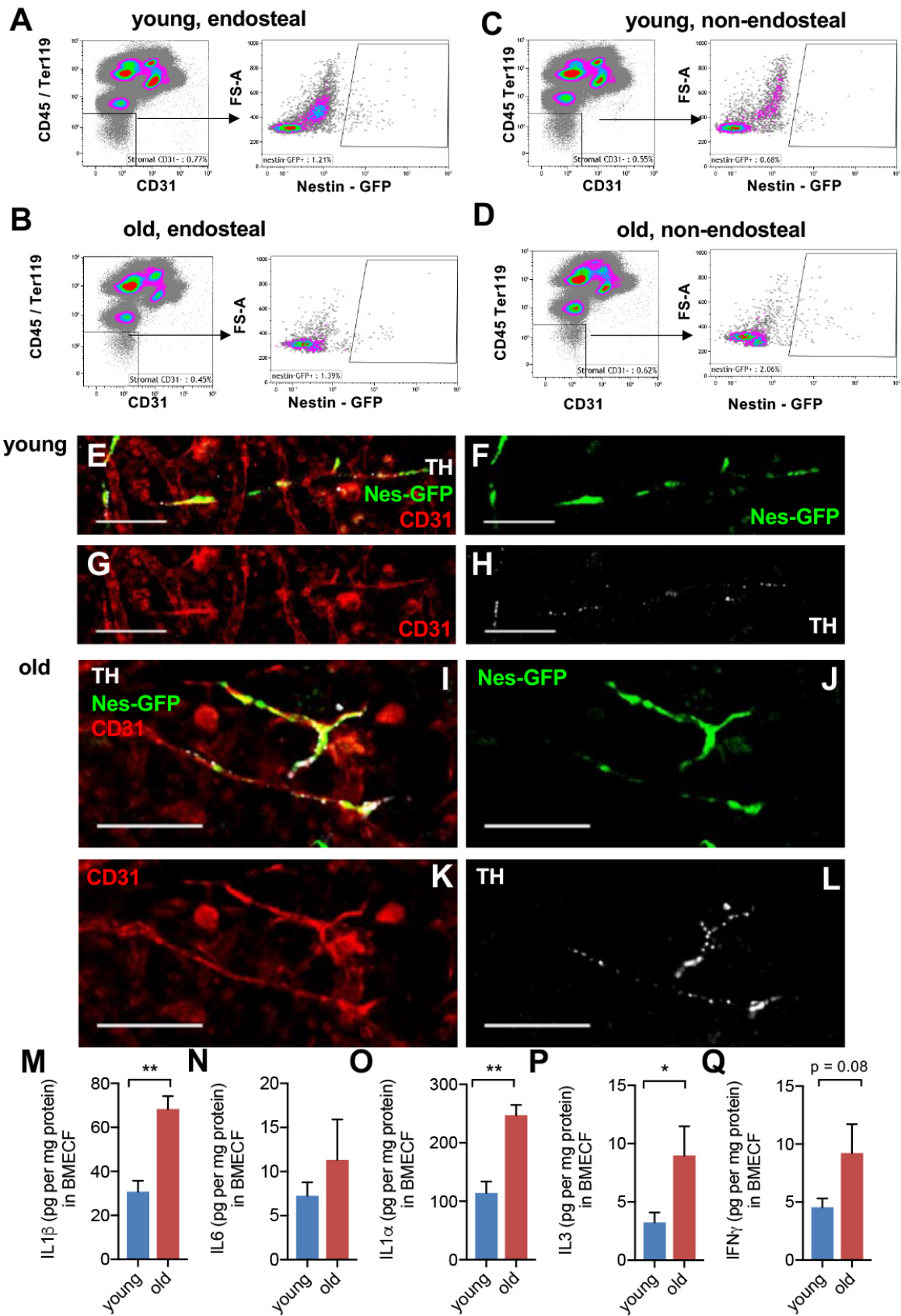
**Remodeling of Bone Marrow Hematopoietic**

**Stem Cell Niches Promotes Myeloid Cell Expansion**

**during Premature or Physiological Aging**

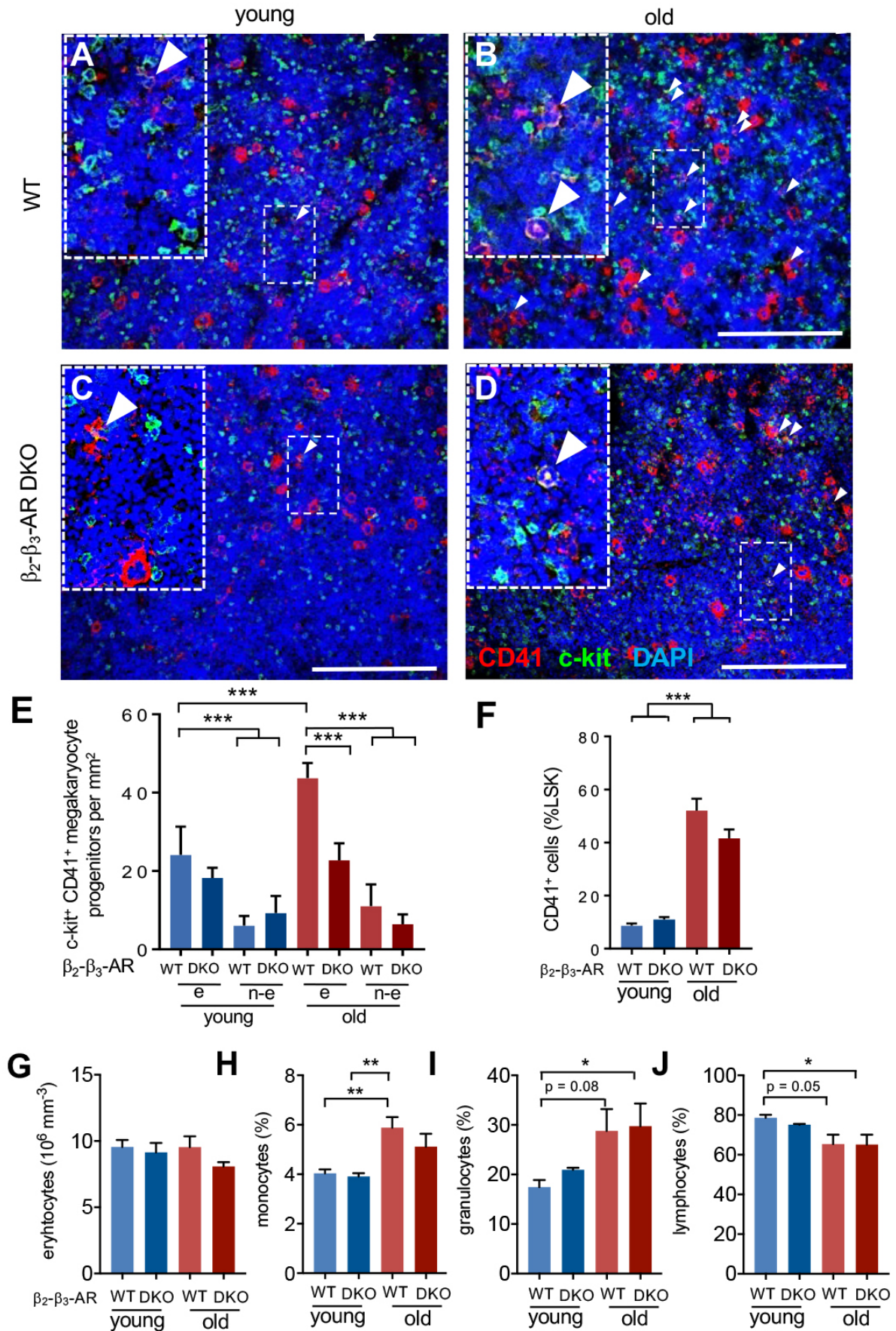
**Ya-Hsuan Ho, Raquel del Toro, José Rivera-Torres, Justyna Rak, Claudia Korn, Andrés García-García, David Macías, Cristina González-Gómez, Alberto del Monte, Monika Wittner, Amie K. Waller, Holly R. Foster, Carlos López-Otín, Randall S. Johnson, Claus Nerlov, Cedric Ghevaert, William Vainchenker, Fawzia Louache, Vicente Andrés, and Simón Méndez-Ferrer**

Figure S1, Related to Figure 1 and Figure 2



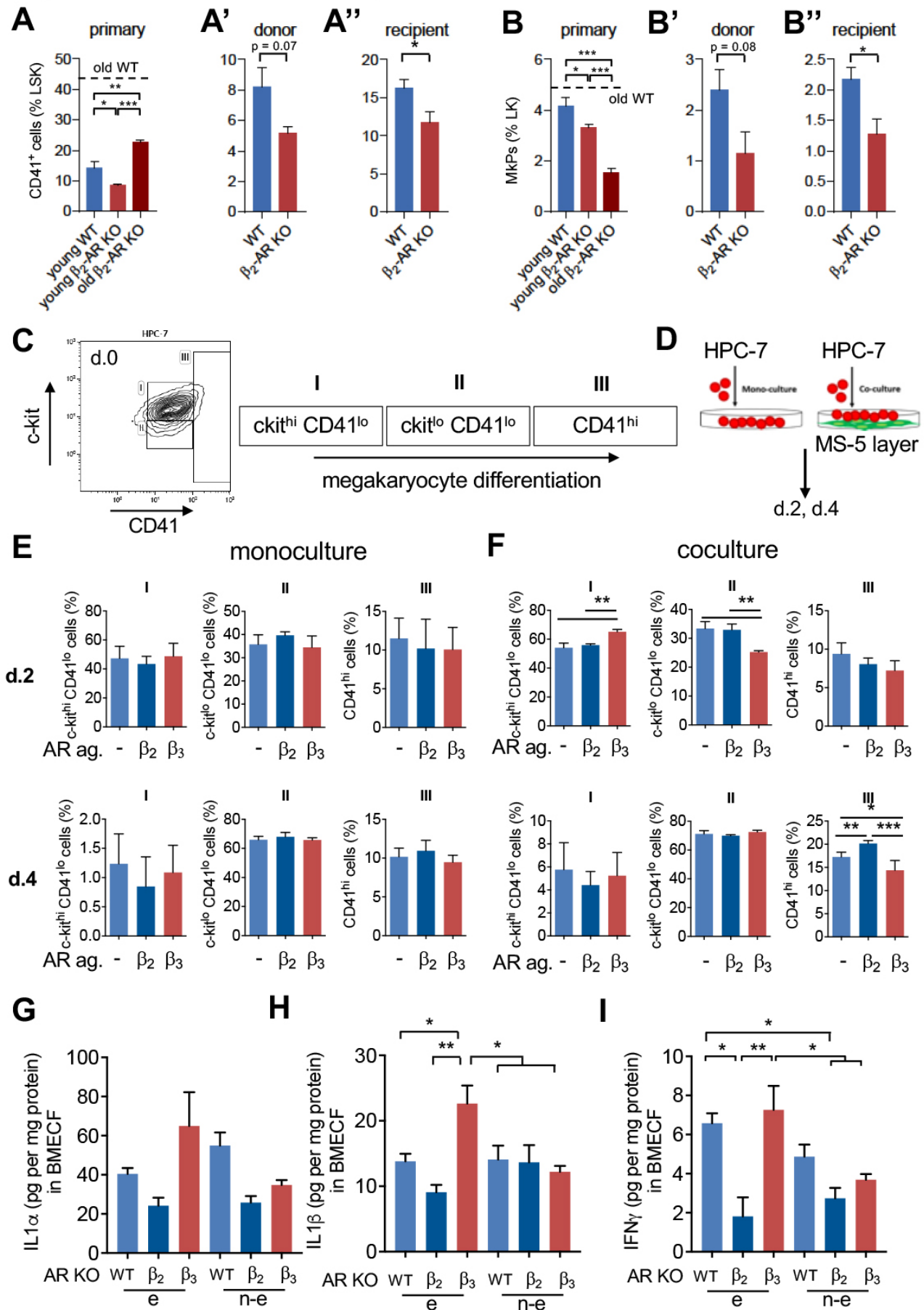
**Figure S1, Related to Figure 1 and Figure 2. Reduction of endosteal niches and expansion of non-endosteal neurovascular niches correlates with increased myelopoietic cytokines during BM aging.** (A-D) Representative flow cytometry diagrams from BM CD45<sup>-</sup> Ter119<sup>-</sup> Nes-GFP<sup>+</sup> cells isolated from (A, B) endosteal and (C, D) non-endosteal BM from (A, C) young and (B, D) old *Nes-gfp* mice. The frequencies of gated population are indicated. (E-L) Additional examples showing the immunofluorescence of tyrosine hydroxylase (TH)<sup>+</sup> sympathetic nerve fibers (white), CD31<sup>+</sup> endothelial cells (red), and GFP<sup>+</sup> cells (green) in the tibial BM of (E-H) young and (I-L) old *Nes-gfp* mice. Scale bar, 100  $\mu$ m. (M-Q) Protein concentration of (M) IL1 $\beta$ , (N) IL6, (O) IL1 $\alpha$ , (P) IL3 and (Q) IFN $\gamma$  in non-endosteal BM extracellular fluid (BMECF) from young WT mice (n = 3) and old WT mice (n = 7). Data are means  $\pm$  SEM. \* p < 0.05; \*\* p < 0.01. Unpaired two-tailed t test.

Figure S2, Related to Figure 3



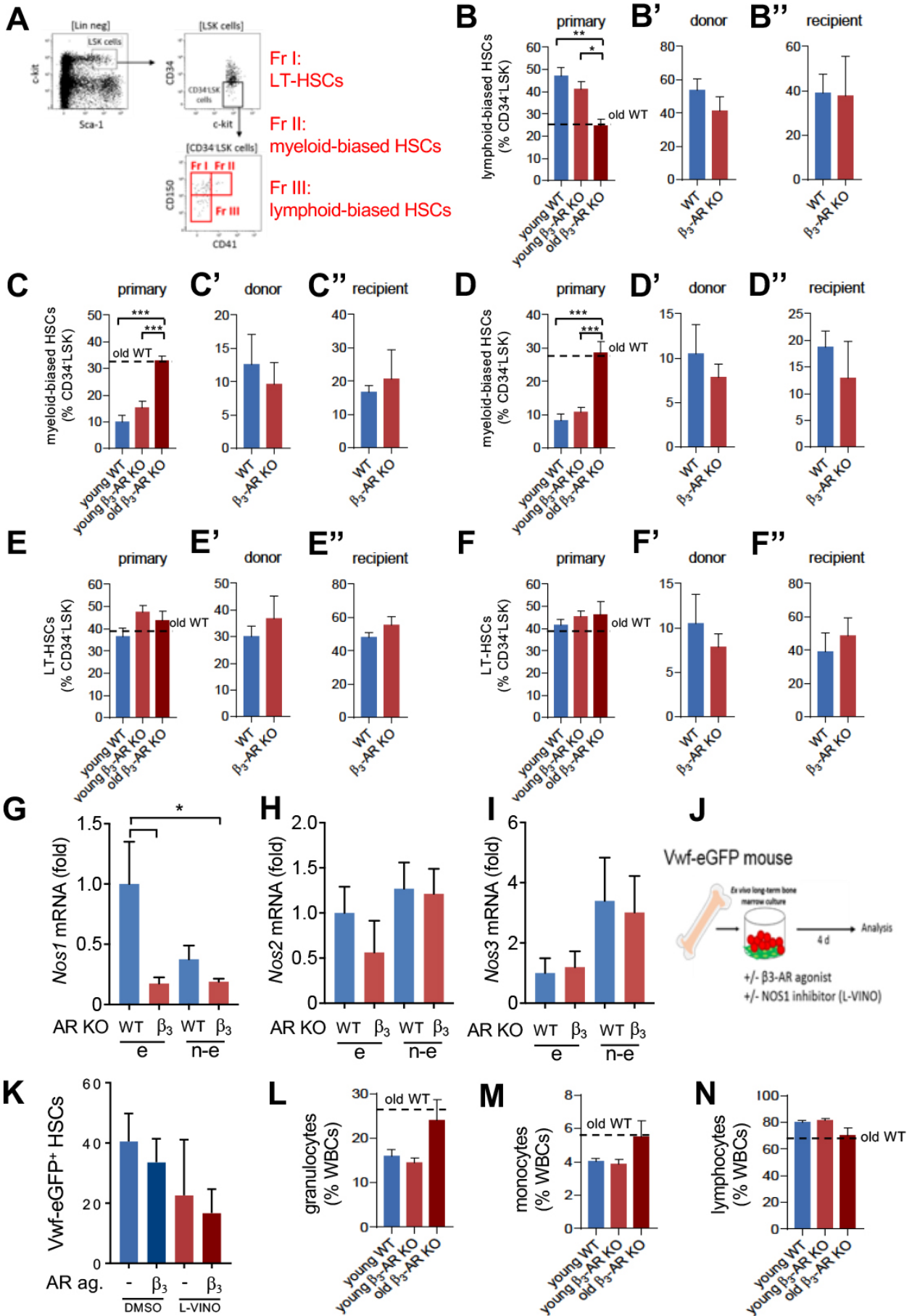
**Figure S2, Related to Figure 3.  $\beta$ -adrenergic signals promote megakaryopoiesis during aging.** (A-D) Representative immunofluorescence staining for CD41 (red) and c-kit (green) in femoral BM sections of WT or  $\beta_2$ - $\beta_3$ -AR DKO mice of different age. Images were taken from the diaphysis regions; c-kit<sup>+</sup>CD41<sup>+</sup> cells are depicted with white arrows. (E) c-kit<sup>+</sup>CD41<sup>+</sup> cells per mm<sup>2</sup> (n = 4 young mice; n = 3 old mice) in endosteal (e) or non-endosteal (n-e) BM areas. Regions within 1/5 marrow width from the bone surface are defined as endosteal (both sides of the bone), while the remaining 3/5 marrow width in the central part are considered as non-endosteal. (F) Frequency of CD41<sup>+</sup> cells in non-endosteal BM Lin<sup>-</sup>Sca-1<sup>+</sup>c-kit<sup>+</sup> (LSK) HSPCs in endosteal BM from young WT mice (n = 7), young  $\beta_2$ - $\beta_3$ -AR DKO mice (n = 7), old WT mice (n = 5), and old  $\beta_2$ - $\beta_3$ -AR DKO mice (n = 4) measured by flow cytometry. (G-J) Peripheral blood counts from young WT mice (n = 8), young  $\beta_2$ - $\beta_3$ -AR DKO mice (n = 8), old WT mice (n = 6) and old  $\beta_2$ - $\beta_3$ -AR DKO mice (n = 7). (G) Erythrocytes. (H-J) Frequencies of (H) monocytes, (I) granulocytes and (J) lymphocytes among white blood cells. Data are means  $\pm$  SEM. \* p < 0.05; \*\* p < 0.01; \*\*\* p < 0.001 (One-way Anova followed by Bonferroni pairwise comparisons).

Figure S3, Related to Figure 4



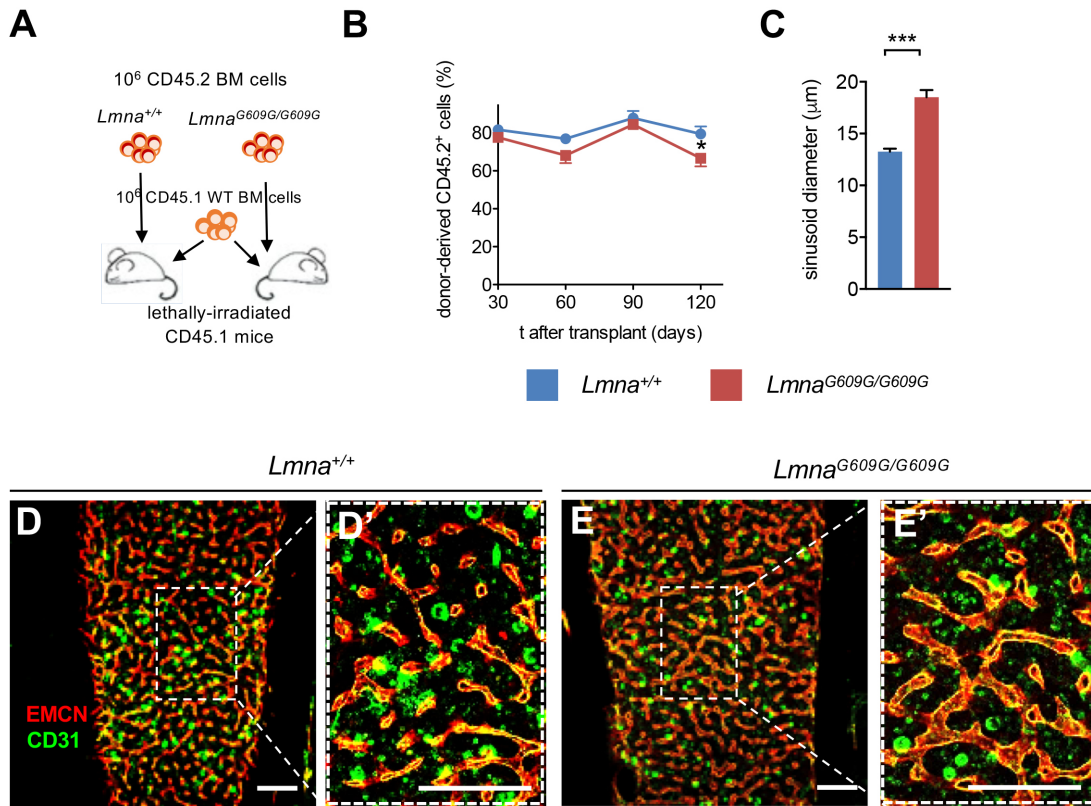
**Figure S3, Related to Figure 4.  $\beta$ -ARs have opposite, stage-divergent and stromal-cell-dependent effects on megakaryocyte differentiation.** (A-B) Frequency of (A, A', A'') CD41<sup>+</sup> myeloid or megakaryocyte progenitors within lin<sup>-</sup>sca-1<sup>+</sup>c-kit<sup>+</sup> (LSK) cells or (B, B', B'') CD150<sup>+</sup>CD41<sup>+</sup> megakaryocyte progenitors (MkPs) within lin<sup>-</sup>c-kit<sup>+</sup> (LK) cells in non-endosteal BM cells of the following mice: (A, B) young WT (A, n = 6; B, n = 3), young *Adrb2*<sup>-/-</sup> (n = 8) or old *Adrb2*<sup>-/-</sup> (n = 4) mice; (A', B') lethally-irradiated WT recipients of WT (n = 5) or *Adrb2*<sup>-/-</sup> (n = 4) BM cells; (A'', B'') lethally-irradiated WT (n = 5) or *Adrb2*<sup>-/-</sup> (n = 4) recipients of WT BM cells. (C) Representative flow cytometry diagram of HPC-7 cells before treatment with cytokines (day 0). Scheme showing the cell populations indicating progressive megakaryocyte commitment: I, ckit<sup>hi</sup>CD41<sup>lo</sup> cells; II, ckit<sup>lo</sup>CD41<sup>lo</sup> cells; III, CD41<sup>hi</sup> cells. Megakaryocyte differentiation trajectory flows from populations I  $\rightarrow$  II  $\rightarrow$  III. (D) Scheme showing the experimental design. HPC-7 cells were cultured alone or co-cultured with MS-5 stromal cells in megakaryocyte differentiation medium. (E-F) Quantification of cell populations I, II and III after 2 or 4 days of treatment with vehicle,  $\beta_2$ -AR agonist or  $\beta_3$ -AR agonist in (E) monoculture or (F) coculture with MS-5 stromal layers (n = 4). (G-I) Concentration of (G) IL1 $\alpha$ , (H) IL1 $\beta$  and (I) IFN $\gamma$  in endosteal (e) or non-endosteal (n-e) BM extracellular fluid (BMECF) from adult WT mice (n = 6), *Adrb2*<sup>-/-</sup> mice (n = 4), or *Adrb3*<sup>-/-</sup> mice (n = 7). Data are means  $\pm$  SEM. \* p < 0.05; \*\* p < 0.01; \*\*\* p < 0.001. (A, B, E-I) One-way Anova followed by Bonferroni pairwise comparisons. (A', A'', B', B'') Unpaired two-tailed t test.

Figure S4, Related to Figure 5



**Figure S4, Related to Figure 5.  $\beta$ 3-AR regulates HSC lineage bias partially through Nos1-dependent NO production.** (A) Representative flow cytometry diagram of HSC populations based on CD41 and CD150 expression. (B) Frequency of CD150<sup>lo/-</sup>CD41<sup>-</sup> lymphoid-biased HSCs in non-endosteal BM CD34<sup>-</sup>LSK cells. (C-F) Frequency of (C-D) CD150<sup>+</sup>CD41<sup>+</sup> myeloid-biased HSCs or (E-F) CD150<sup>+</sup>CD41<sup>-</sup> LT-HSCs in (C, E) endosteal or (D, F) non-endosteal BM CD34<sup>-</sup>LSK cells from the following mice: (B, C, D, E, F) young WT (n = 7), young *Adrb3*<sup>-/-</sup> (n = 7) or old *Adrb3*<sup>-/-</sup> (n = 5) mice; (B', C', D', E', F') lethally-irradiated WT recipients of WT (n = 5) or *Adrb3*<sup>-/-</sup> (n = 5) BM cells; (B'', C'', D'', E'', F'') lethally-irradiated WT (n = 4) or *Adrb3*<sup>-/-</sup> (n = 3) recipients of WT BM cells. (G-I) mRNA levels (fold) of (G) *Nos1* (H) *Nos2* and (I) *Nos3* in the endosteal (e) or non-endosteal (n-e) BM of adult WT mice (n = 6) and  $\beta$ 3-AR KO mice (n = 7). (J) Scheme of long-term BM culture from *Vwf-eGFP* mice. (K) Number of lin<sup>-</sup>sca-1<sup>+</sup>c-kit<sup>+</sup>CD34<sup>-</sup>CD48<sup>-</sup>CD150<sup>+</sup>Vwf-eGFP<sup>+</sup> platelet-biased HSCs in primary BM culture from *Vwf-eGFP* mice treated with  $\beta$ 3-AR agonist (BRL37344, 10  $\mu$ M), *Nos1* inhibitor (L-VINO, 100  $\mu$ M) or vehicle for 4 days (n = 8). (L-N) Frequency of (L) granulocytes, (M) monocytes and (N) lymphocytes in white blood cells (WBCs) in young WT (L, N, n = 10; M, n = 8), young *Adrb3*<sup>-/-</sup> (n = 4) or old *Adrb3*<sup>-/-</sup> (n = 6) mice. Data are means  $\pm$  SEM. \* p < 0.05; \*\* p < 0.01. (B', B''-F', F'') Unpaired two-tailed *t* test. (B-F, G-N) One-way Anova followed by Bonferroni pairwise comparisons.

## Figure S5, Related to Figure 6



**Figure S5, Related to Figure 6. Characterization of hematopoiesis and BM vasculature in HGPS mice.** (A) Scheme of competitive BM transplantation. (B) Frequency of CD45.2<sup>+</sup> donor-derived hematopoietic cells in peripheral blood of recipient mice 30, 60, 90 and 120 days after lethal irradiation and transplantation with 10<sup>6</sup> BM cells from WT (blue) or *Lmna*<sup>G609G/G609G</sup> (red) mice, together with 10<sup>6</sup> competitor BM cells from CD45.1 C57BL/6 mice. (C) Quantification of sinusoidal (EMCN<sup>+</sup> vasculature) diameter in each group of mice. (D, E) Representative immunofluorescence of CD31 (green) and EMCN (red) in thick femoral BM sections from adult WT mice (*Lmna*<sup>+/+</sup>; n = 7) and *Lmna*<sup>G609G/G609G</sup> mice (n = 7). Scale bar, 200 μm. (D', E') Insets of D and E. Scale bar, 100 μm. (B-C) Data are means ± SEM. \* p < 0.05; \*\*\* p < 0.001 (unpaired two-tailed t test).

## Figure S6, Related to Figure 6 and Figure 7

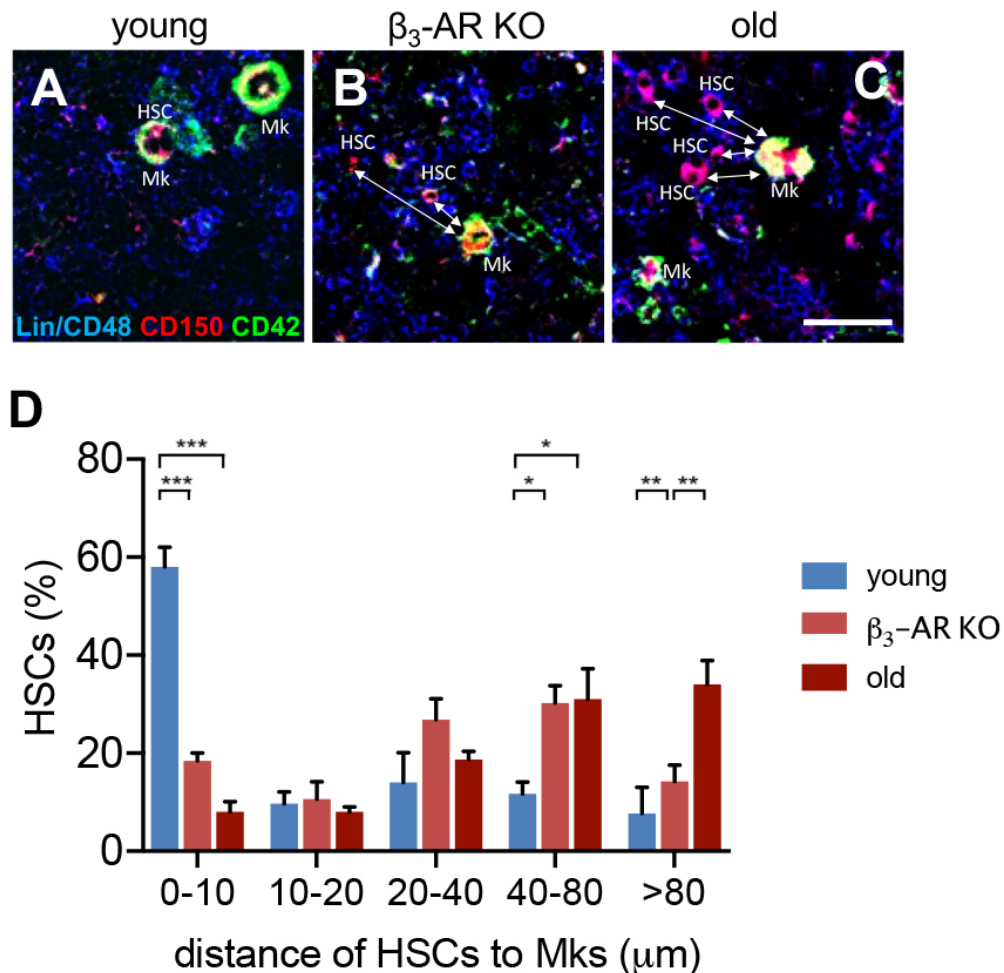


**Figure S6, Related to Figure 7. Decreased HSC-megakaryocyte interactions in adult  $\beta_3$ -AR KO mice resemble aged WT mice.** (A-D) Representative immunofluorescence (A-C) and distribution (D) of BM CD150<sup>+</sup> (red) HSCs (negative for mature hematopoietic lineage markers, blue) adjacent (asterisks) or nonadjacent (arrows) to CD42<sup>+</sup> (green) megakaryocytes in femoral BM sections of young WT mice (n = 3), adult *Adrb3*<sup>-/-</sup> mice (n = 5) and old WT mice (n = 3). Scale bar, 50  $\mu$ m. Data are means  $\pm$  SEM. \* p < 0.05; \*\* p < 0.01; \*\*\* p < 0.001 (Two-way Anova and Bonferroni pairwise comparisons).

Figure S7, Related to Figure 6

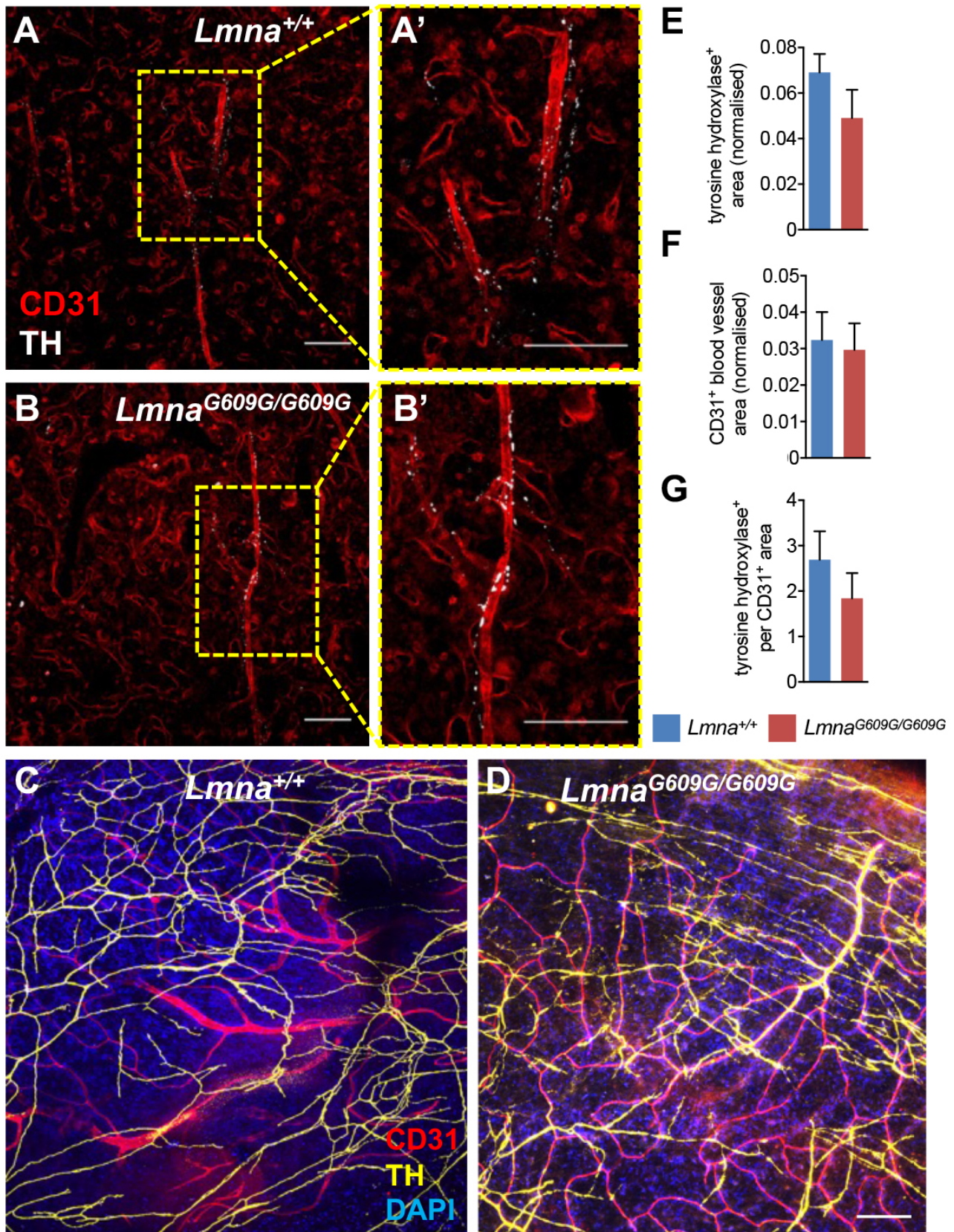


**Figure S7, Related to Figure 6 and 7. BM noradrenergic innervation is not reduced in a mouse model of premature aging.** (A-D) Whole-mount immunofluorescence staining of tyrosine hydroxylase (TH)<sup>+</sup> sympathetic nerve fibers (A, B, white; C, D, yellow) and CD31<sup>+</sup> endothelial cells (red) in the femoral BM (A, B) and skull (C, D) of (A, C) adult WT mice (*Lmna*<sup>+/+</sup>; n = 6) and (B, D) *Lmna*<sup>G609G/G609G</sup> mice (n = 7). A', B', insets of A and B. Scale bar, 100 μm (A, B), 200 μm (C, D). (E) Quantification of the area covered by TH<sup>+</sup> fibers in the skull. (F) Quantification of the area covered by CD31<sup>+</sup> endothelial cells in the skull. (G) Ratio of the area of TH<sup>+</sup> fibers to CD31<sup>+</sup> endothelial cells in the skull. Data are means ± SEM.